An investigation of some effects of drifts and magnetic field direction in the scrape-off layer and divertor of tokamak plasmas

W. M. Stacey[a)]
Fusion Research Center, Georgia Institute of Technology, Atlanta, Georgia 30332, USA

(Received 19 December 2008; accepted 25 February 2009; published online 3 April 2009)

Various effects of particle drifts in the scrape-off layer (SOL) and divertor of tokamaks have been calculated. The predictions are consistent with several experimentally observed phenomena, e.g., the double reversal of parallel ion velocity in the SOL and the enhanced core penetration of argon injected into the divertor when the grad-B ion drift is into, rather than away from, the divertor. Other interesting phenomena, such as the structure of the parallel current flowing in the SOL and the reversal of the sign of the electrostatic potential in the SOL when the toroidal field direction is reversed, are also predicted. © *2009 American Institute of Physics*. [DOI: 10.1063/1.3099604]

I. INTRODUCTION

The physics of the plasma outside the last closed flux surface, or separatrix, in the edge of diverted tokamak plasmas is a subject of current research interest, both because of the intrinsic importance of the physics of the scrape-off layer (SOL) and divertor for heat removal and particle exhaust in tokamaks, but also because of the growing evidence of the influence of divertor and SOL physics on the physics of the edge pedestal region and hence on the performance parameters of the "core" plasma.

The diverse thermodynamic, electrical, magnetic, atomic physics, etc., phenomena that interact to determine the properties of the SOL and divertor make this plasma edge region both a rich source of complex physical phenomena and a computational challenge. Pioneering computational and experimental studies (e.g., Refs. 1–6) have identified the importance of cross-field drifts and currents in understanding experimental phenomena in the divertor and SOL. In particular, various plasma edge phenomena have been found to be quite sensitive to the direction of the ion grad-B drift, toward or away from the divertor. This observation of the strong impact of drifts and magnetic field direction on divertor and SOL plasma parameters has motivated the computational investigation presented in this paper.

This paper presents an analysis of the effect of magnetic field direction, acting through curvature, grad-B and $E\times B$ drifts, on the divertor and SOL parameters for a model problem representative of a DIII-D (Ref. 7) *H*-mode discharge. The particular objective of these calculations was elucidation of the mechanisms by means of which particle drifts and the direction of the toroidal magnetic field affect the densities, temperatures, flows, currents, and electric fields in the divertor and SOL. The investigations were informed by recently observed new experimental phenomena.

The calculation model is described in Sec. II, the calculated effects of grad-B, curvature and $E\times B$ drifts on divertor and SOL plasma parameters for different toroidal magnetic field directions are discussed in Sec. III, and a summary is provided in Sec. IV.

[a)]Electronic mail: weston.stacey@nre.gatech.edu.

II. CALCULATION MODEL

In principle, such an investigation as is presented in this paper could be carried out by solving directly the governing equations for the flows, currents, densities, temperatures, electric fields, etc., in the SOL and divertor. However, such an approach leads to practical difficulties, as found and circumvented by previous workers (e.g., Refs. 1 and 2).

One difficulty is that the resulting calculation of some important quantities is of the form of a small difference of two or more large terms, leading to numerical problems in achieving a solution. This has led previous workers to manipulation of the equations involved to analytically eliminate the larger parts of these terms which can be canceled; e.g., Rozhansky *et al.*[2] state that "To avoid numerical problems while the code is running, in several places divergence-free terms in the particle and current balance equations are canceled analytically." These authors go on to show that the divergence-free part of the diamagnetic velocities are proportional to gradients in the magnetic field and state "Physically, velocity Eq. (6) *for the non-divergence-free part of the diamagnetic velocities* represents vertical guiding centre drift of ions caused by ∇B."

Rozhansky *et al.*[2] proceed to evaluate these non-divergence-free parts of the diamagnetic flow numerically by differentiating the magnetic field, which introduces a second difficulty—the requirement for a very accurate representation of the magnetic field geometry. Rognlien *et al.*[1] avoid this second difficulty by using analytical expressions for the divergence-free leading order diamagnetic and $E\times B$ drifts and then using analytical expressions for the higher order grad-B and curvature drifts (rather than numerically differentiating the local magnetic field), thus avoiding the requirement for a very accurate representation of the local field geometry. They represent the ion grad-B drift as "downward toward the *X*-point," i.e., as vertical, and adopt a radial-poloidal coordinate system.

We take into account the experience of these two previous sets of authors[1,2] in formulating a solution procedure for the flows, currents, densities, etc., in the SOL and divertor. Specifically, we use the leading order divergence-free diamagnetic velocity to calculate particle flows, but use the analytical vertical grad-B (and curvature) drift expression to ac-

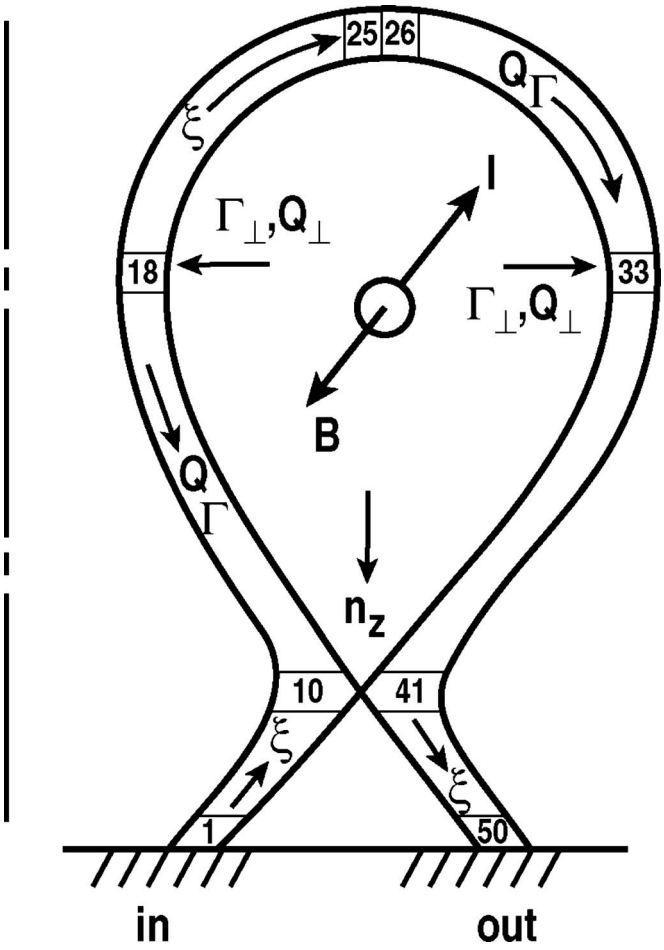

FIG. 1. Geometric model of SOL-divertor. (Reprinted from Ref. 8.)

count for the contribution of the diamagnetic flows to the divergence of the current, and we use a radial-poloidal geometry but with the poloidal component mapped onto a "pseudoparallel" coordinate to facilitate the description of the calculation. We further approximate the radial calculations in order to reduce the computational intensity of the calculation.

A. Geometrical model

The calculation is formulated in the "radial-poloidal" strip of plasma outside the separatrix shown in Fig. 1. For convenience in representing the divertor channels and in describing the geometric location within the SOL, the poloidal coordinate is mapped onto a pseudoparallel coordinate. The plasma outside the separatrix is modeled as a "stack" of two-dimensional (2D) strips, or "ribbons," that spiral about the core plasma (q times between X-points) following the magnetic field lines from the inner to the outer divertor target plate. Nonuniformities in the magnetic geometry are represented by particle "drifts" to account for the effects of field gradients and curvature while retaining a simple computational geometry. The parameter ξ designates the distance "along the field lines" from the inner ($\xi=\xi_{in}$) to the outer ($\xi=\xi_{out}$) divertor targets.

B. Radial transport

The 2D transport problem in this strip is reduced to one-dimensional by writing the divergence of the particle and heat fluxes as, e.g., for the particle flux $\nabla\bullet\Gamma=d\Gamma/d\xi+d\Gamma/dr$ and approximating the radial term by following experiment observation to assume that the density (and temperature) exponentially attenuate radially outward from the separatrix, $n=n_{sep}\exp(-r/\Delta_n)$ in the SOL. Requiring continuity across the separatrix of the ion particle flux $\Gamma_\perp^{sep}$ from the core into the SOL with a diffusive radial particle flux in the SOL $\Gamma_r=-D_\perp dn/dr$ identifies $\Delta_n=n_{sep}D_\perp/\Gamma_\perp^{sep}$. At the outer edge of the SOL, which is taken as a distance $\varepsilon\Delta_n$ outside the separatrix, the radially outward ion flux lost from the SOL plasma is $\Gamma_\perp^{sol}=D_\perp\Delta_n^{-1}n_{sep}e^{-\varepsilon}$. This leads to an approximation $d\Gamma/dr\approx(\Gamma_\perp^{sol}-\Gamma_\perp^{sep})/\Delta_n=-(\Gamma_\perp^{sep}/\Delta_n)(1-e^{-\varepsilon})\equiv-\Gamma_\perp/\Delta_n$ for the radial contribution to the divergence of the particle flux. In this work, $\varepsilon=1$ is used in the SOL (between X-points) and $\varepsilon=3$ is used in the divertor channels to reflect the expansion of field line separation.

In the divertor channel, the density, and temperature distributions outside the separatrix are observed to first increase sharply with "radial" distance from the separatrix, peak, and then attenuate exponentially with further distance from the separatrix. This observation is indicative of a diffusive type loss both inward into the private flux region and outward toward the divertor chamber walls. There is no incident ion particle flux from the core, of course, so only the radial transport loss term $-D_\perp n/\Delta_n^2$ is present in the divertor.

A similar argument can be used to approximate the radial component of the divergence of the heat flux, Q. When it is further assumed that parallel heat flux is dominated by electron heat conduction, $Q\approx\kappa_\parallel dT/d\xi=\kappa_0T^{5/2}dT/d\xi$, the resulting approximation of radial transport is $dQ/dr\approx-(Q_\perp^{sep}/\Delta_E)(1-e^{\varepsilon})\equiv-Q_\perp/\Delta_E$, where $\Delta_E=2\chi_\perp n_{sep}T_{sep}/7Q_\perp^{sep}$, with $Q_\perp^{sep}$ representing the heat flux from the core flowing across the separatrix into the SOL. In the divertor channel only the transport loss term $-nT\chi_\perp/\Delta_E^2$ is present.

Thus, the radial transport is represented by the parameters Δ_n and Δ_E, which can either be determined from experimental measurements or calculated from theoretical models for radial transport. The Bohm transport coefficients $D_\perp=T/16eB$, $\chi_\perp=5T/32eB$ are often used, but any other diffusive transport model can equally well be used. Representation of nondiffusive radial transport (e.g., "blob transport") would probably require an extension of this formalism, but this is beyond the scope of this paper. Since radial transport is poorly understood at present, the use of experimentally observed gradient scale lengths would seem preferable in the interpretation of experiments.

C. Temperature, density, and velocity distributions

The parallel energy balance equation solved for the heat flux Q in the SOL and divertor in a strip running from the inner divertor target plate around the plasma in a clockwise positive direction to the outer diver plate, as shown in Fig. 1, is

$$\frac{dQ}{d\xi} = \frac{Q_\perp}{\Delta_E} - n_z n_e L_z - E_{\rm ion} n_e n_o \langle \sigma v \rangle_{\rm ion} + f I_{\rm ion} n_i n_e \langle \sigma v \rangle_{\rm rec} - \frac{3}{2} n_i n_o^c \langle \sigma v \rangle_{\rm cxel} + j_\parallel E_\parallel \equiv \frac{Q_\perp}{\Delta_E} - P_{\rm rad} - P_{\rm at} + P_\Omega, \quad (1)$$

where $Q_\perp$ is the perpendicular heat flux across the separatrix into the SOL (reduced by the radial transport heat loss from the SOL), the second term represents impurity radiation (and bremsstrahlung) cooling, and the last three atomic physics terms represent ionization cooling, recombination heating, and charge-exchange plus elastic scattering cooling of the plasma. The sheath boundary conditions specify a heat flux into the inner and outer divertor plates

$$Q_{\rm in} = -n_{\rm in} c_{s,{\rm in}} T_{\rm in} \gamma_{\rm in}, \quad Q_{\rm out} = n_{\rm out} c_{s,{\rm out}} T_{\rm out} \gamma_{\rm out}, \quad (2)$$

where

$$\gamma = \frac{2T_i}{T_e} + \frac{2}{1-\delta} + \frac{1}{2}\ln\left(\frac{(1-\delta)m_i/m_e}{2\pi(1+T_i/T_e)}\right) \quad (3)$$

is the sheath coefficient and δ is the secondary electron emission coefficient.

The parallel particle balance equation is

$$\frac{d\Gamma}{d\xi} = \frac{\Gamma_\perp}{\Delta_n} + n_e(n_o \langle \sigma v \rangle_{\rm ion} - n_i \langle \sigma v \rangle_{\rm rec}) \equiv \frac{\Gamma_\perp}{\Delta_n} + n_e(\nu_{\rm ion} - \nu_{\rm rec}), \quad (4)$$

where $\Gamma_\perp$ is the perpendicular particle flux from the core across the separatrix into the SOL (reduced by the radial particle loss) and "ion" and "rec" refer to ionization and recombination. The sheath boundary conditions specify that the particle fluxes into the target plates are

$$\Gamma_{\rm in} = -n_{\rm in} c_{s,{\rm in}}, \quad \Gamma_{\rm out} = n_{\rm out} c_{s,{\rm out}}, \quad (5)$$

where c_s is the sound speed. In both Eqs. (2) and (5), the minus sign indicates that the flux is into the plate at the inner divertor target in the negative sense of the parallel coordinate ξ. These incident ions are recycled as neutral atoms and molecules, with the latter being dissociated immediately and transported as low energy atoms until they have a charge-exchange or elastic scattering collision, upon which they are combined with the higher energy reflected neutrals and transported throughout the divertor and SOL and inward across the separatrix.[9]

Solving Eqs. (1) and (2) for

$$Q(\xi) = -n_{\rm in} c_{s,{\rm in}} T_{\rm in} \gamma_{\rm in} + \int_{\xi_{\rm in}}^{\xi} \left(\frac{Q_\perp}{\Delta_E} - P_{\rm rad} - P_{\rm at}\right) d\xi' \quad (6)$$

and assuming that parallel heat transport is dominated by classical electron heat conduction $Q(\xi) \approx q(\xi) = -\kappa_0 T^{5/2} dT/d\xi = -(2/7)\kappa_0 dT^{7/2}/d\xi$ leads to a solution for the temperature distribution in terms of the heat flux calculated from Eq. (6)

$$T^{7/2}(\xi) = T_{\rm in}^{7/2} - \frac{7}{2\kappa_0}\int_{\xi_{\rm in}}^{\xi} Q(\xi')d\xi' = T_{\rm in}^{7/2} - \frac{7}{2\kappa_0}\int_{\xi_{\rm in}}^{\xi}\left[-n_{\rm in} c_{s,{\rm in}} T_{\rm in}\gamma_{\rm in} + \int_{\xi_{\rm in}}^{\xi'}\left(\frac{Q_\perp}{\Delta_E} - P_{\rm rad} - P_{\rm at}\right)d\xi''\right]d\xi'. \quad (7)$$

The parallel momentum balance equation can be written, neglecting viscosity, as

$$\frac{dM}{d\xi} \equiv \frac{d}{d\xi}(2p + nmv^2) = -m(\nu_{\rm cxel} + \nu_{\rm ion})\Gamma \equiv -m\nu_{\rm mom}\Gamma \quad (8)$$

and integrated to solve for

$$M(\xi) = M(\xi_{\rm in}) - \int_{\xi_{\rm in}}^{\xi} m\nu_{\rm mom}(\xi')\Gamma(\xi')d\xi' = 4n_{\rm in}T_{\rm in} - \int_{\xi_{\rm in}}^{\xi} m\nu_{\rm mom}(\xi')\Gamma(\xi')d\xi'. \quad (9)$$

$M(\xi)$ can then be equated to $(2p+nmv^2)$ to obtain a quadratic equation in $n(\xi)$

$$[2p(\xi) + n(\xi)mv^2(\xi)] \equiv [2n(\xi)T(\xi) + m\Gamma^2(\xi)/n(\xi)] = M(\xi), \quad (10)$$

which yields a solution for the plasma ion density

$$n(\xi) = \frac{M(\xi)}{4T(\xi)}[1 \pm \sqrt{1 - 8mT(\xi)\Gamma^2(\xi)/M^2(\xi)}] \quad (11)$$

that can be used in the definition of Γ to obtain the plasma flow velocity

$$v(\xi) = \Gamma(\xi)/n(\xi). \quad (12)$$

The sheath boundary condition on the parallel flow velocity is

$$v(\xi_{\rm in}) = -c_{s,{\rm in}} \equiv -\sqrt{\frac{2T_{\rm in}}{m}}, \quad v(\xi_{\rm out}) = c_{s,{\rm out}} \equiv \sqrt{\frac{2T_{\rm out}}{m}}. \quad (13)$$

In all calculations to date, the larger value obtained using the + sign in Eq. (11) has been of the magnitude observed in experiment, but the smaller value has not been physically unreasonable, perhaps implying the existence of a lower density divertor regime.

D. Electrostatic potential

The electrostatic potential satisfies the electron parallel momentum balance equation

$$\frac{d\phi}{d\xi} = \frac{0.71}{e}\frac{dT}{d\xi} + \frac{1}{ne}\frac{dp}{d\xi} - \frac{j_\parallel}{\sigma_\parallel}, \quad (14)$$

which can be integrated to obtain

$$\phi(\xi) = \phi_{\rm in} + \frac{1.71}{e}[T(\xi) - T_{\rm in}] + \int_{\xi_{\rm in}}^{\xi} \frac{T(\xi')}{en(\xi')}\frac{dn(\xi')}{d\xi'}d\xi' - \int_{\xi_{\rm in}}^{\xi} \frac{j_{\parallel}(\xi')}{\sigma_{\parallel}(\xi')}d\xi', \tag{15}$$

where the potential just in front of the target plate is given by the current-potential sheath relation between the potential just in front of the plate ($\phi_{\rm in,out}$) and the current ($j_{\rm pl}^{\rm in,out}$) into the plate

$$\phi_{\rm in} = -\frac{T_{\rm in}}{e}\ln\left[\frac{\sqrt{m_i/\pi m_e}(1-\delta)}{1 - j_{\rm pl}^{\rm in}/n_{\rm in}ec_{\rm si,in}}\right],$$
$$\phi_{\rm out} = -\frac{T_{\rm out}}{e}\ln\left[\frac{\sqrt{m_i/\pi m_e}(1-\delta)}{1 - j_{\rm pl}^{\rm out}/n_{\rm out}ec_{\rm si,out}}\right], \tag{16}$$

where $\sigma_{\parallel} = 2n_e e^2\tau_e/m_e$, $\tau_e = 3\sqrt{m_e}T^{3/2}/4\sqrt{2\pi}n_e \ln\Lambda e^4$.

It is noted that although the "standard" procedure[1,2] for calculating the potential in the SOL-divertor region involves substituting the parallel current from the parallel momentum balance of Eq. (14) into the current continuity condition $\nabla\cdot\mathbf{j}=0$, the second entry of Ref. 2 demonstrates that a one-dimensional calculation of the poloidal (or parallel) dependence of the potential (such as developed in this section) can provide an accurate result.

It is further noted that any effect of ion orbit loss[10] on the calculation of the electrostatic potential is not included in this model.

E. Parallel current

The net current density into the target plates is given by the sum of the ion current density $nec_{\rm si}$ and the electron current density, $(1/4)n(-e)\bar{c}_e e^{e\phi/T}$ for a Maxwellian distribution,

$$j_{\rm pl}^{\rm in} = ne\left[c_{\rm si} - \frac{1}{4}\bar{c}_e e^{e\phi/T_e}\right], \tag{17}$$

where $\bar{c}_e = (8T_e/\pi m_e)^{1/2}$ is the average electron speed for a Maxwellian distribution.

The current density must be divergence-free,

$$\nabla\cdot\mathbf{j} \equiv \frac{dj_{\parallel}}{d\xi} + \frac{dj_{\perp}}{d\ell_{\perp}} + \frac{dj_r}{dr} = 0, \tag{18}$$

which may be solved for

$$j_{\parallel}(\xi) = -j_{\rm pl}^{\rm in} - \int_{\xi_{\rm in}}^{\xi}\left[\frac{dj_{\perp}}{d\ell_{\perp}} + \frac{dj_r}{dr}\right]d\xi'. \tag{19}$$

The minus sign in front of the first term on the right results from the fact that Eq. (17) specifies the current into the inner divertor plate, while the positive sense of the current in this model is out of the inner divertor plate (but into the outer divertor plate); i.e., $j_{\parallel}(\xi_{\rm in}) = -j_{\rm pl}^{\rm in}$.

These cross-field currents are driven by grad-B and curvature drifts, as discussed in the following section. They are not driven by $E\times B$ drifts, which are the same for ions and electrons and hence do not produce currents to leading order (neglecting finite Larmour radius effects). The diamagnetic currents have been shown to be almost divergence-free,[1,2,5,11,12] except for small terms related to the nonuniformity in B, which (following Ref. 1) are treated in terms of the grad-B and curvature drifts. The divergent part of the diamagnetic current has been shown to correspond to the vertical drift current due to grad-B and curvature.[2] Cross-field currents also may be driven by cross-field transport, viscosity and other mechanisms that have different effects on ions and electrons, but these mechanisms have been found[1,2] to provide smaller contributions and are not considered at present.

F. Grad-B and curvature drifts

The grad-B and curvature drifts are

$$\upsilon_{\nabla B} = \frac{T}{e}\frac{\mathbf{B}\times\nabla B}{B^3} \approx \frac{T}{eRB}\mathbf{n}_z,$$
$$\upsilon_c = -\frac{m\upsilon_{\parallel}^2}{e}\frac{\mathbf{B}\times\mathbf{R}}{B^2R^2} \approx \frac{m\upsilon_{\parallel}^2}{eRB}\mathbf{n}_z, \tag{20}$$
$$\upsilon_B \equiv \upsilon_{\nabla B} + \upsilon_c \approx \frac{3T}{eRB}\mathbf{n}_z,$$

where $\mathbf{n}_z$ is a unit vector in the vertical direction, up or down depending on the direction of $\mathbf{B}$, and $\upsilon_{\parallel}\approx\upsilon_{\rm th}$. The drifts are in opposite directions for ions and electrons because of the charge sign difference, producing a current

$$\mathbf{j}_B = 2ne\boldsymbol{\upsilon}_B \approx \frac{6nT}{BR}\mathbf{n}_z. \tag{21}$$

At this point, a specific current and magnetic field configuration is adopted for the purpose of description, as shown in Figs. 1–4. For this configuration, the vertical unit vector $\mathbf{n}_z$ is directed downward. Thus, the radial drift currents are radially inward from the SOL into the core in the upper hemisphere ($0\le\theta\le\pi$) and radially outward from the core into the SOL in the lower hemisphere ($\pi\le\theta\le 2\pi$), as indicated in Fig. 2.

The ion grad-B and curvature drifts also produce a poloidal particle drift which is represented in the "parallel" coordinate system as

$$\Gamma_{\nabla B}^{\parallel} = (\mathbf{n}_{\parallel}\cdot\mathbf{n}_z)\Gamma_{\nabla B}^{z} = \left(\frac{B_\theta}{B}\cos\theta\right)\frac{3nT}{eBR}, \tag{22}$$

which is downward in both the inner and outer SOLs and divertors, as indicated in Fig. 2. Here, the angle θ is with respect to the outboard midplane. In the divertor, $\cos\theta$ is replaced by $\sin\alpha$, where α is the angle of incidence with respect to the horizontal of the separatrix, as illustrated in Fig. 2.

Using Eq. (21) to evaluate the radial drift current in Eq. (19) and adding the poloidal drift current from Eq. (22) provides an equation for the resulting parallel current in the SOL as a result of the divergence of the radial grad-B and curvature drift currents plus the poloidal drift current

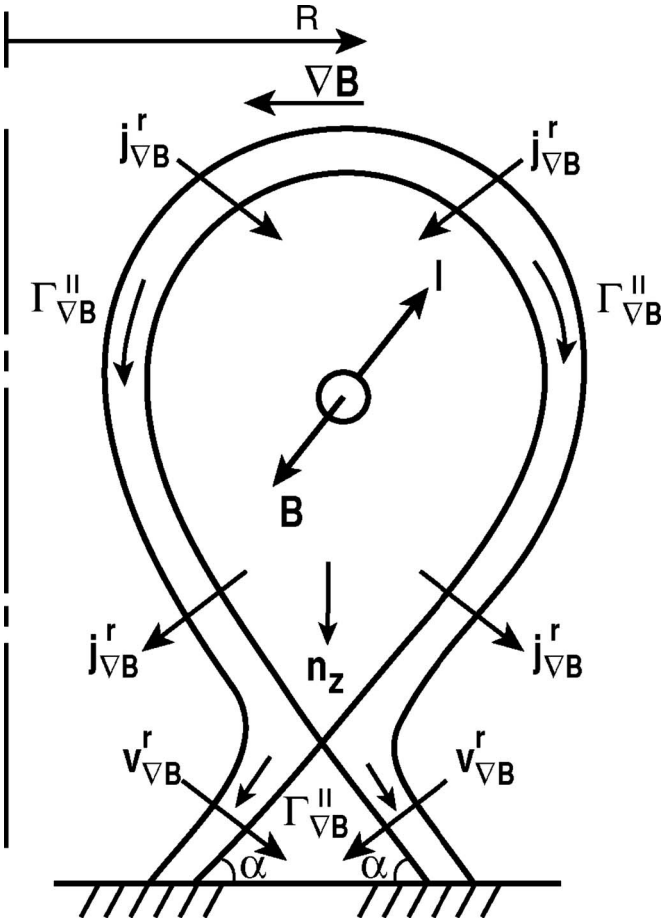

FIG. 2. Schematic illustration of direction of radial and parallel components of vertical [downward for $B(-)$ toroidal magnetic field direction] grad-B and curvature drifts. (Reprinted from Ref. 8.)

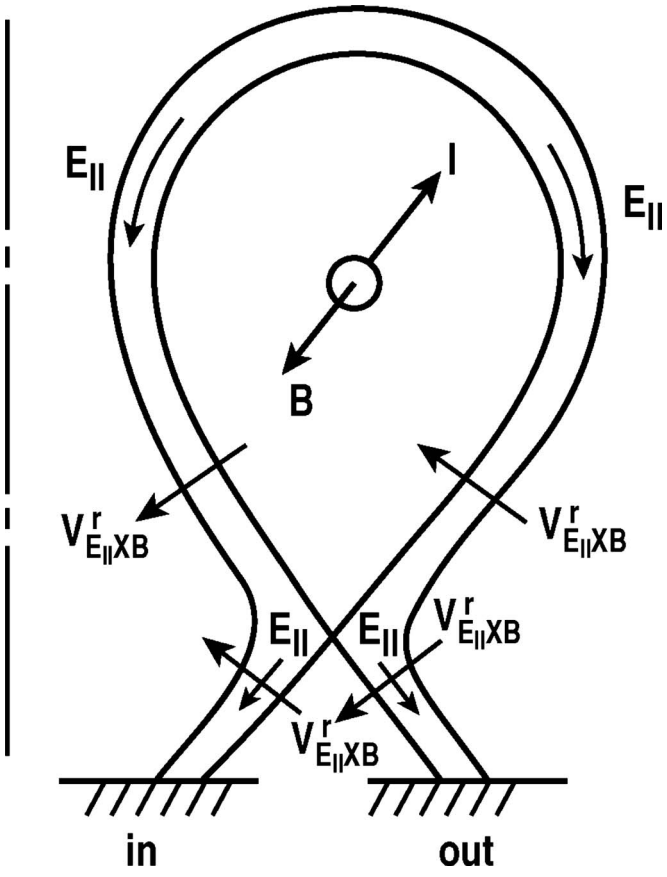

FIG. 3. Schematic of direction of parallel electrostatic field and associated radial $E\times B$ drifts for electrostatic potential increasing from divertor target to SOL crown and $B(-)$ toroidal magnetic field direction.

$$j_{\parallel}(\xi) = j_{\parallel}(\xi_{\rm in}) + \int_{\xi_{\rm in}}^{\xi} \left[\frac{6n(\xi')T(\xi')[\Delta_n^{-1} + \Delta_T^{-1}]}{RB} (\mathbf{n}_r \cdot \mathbf{n}_z) \right] d\xi' + 2e\Gamma^{\parallel}_{\nabla B} \equiv j_{\parallel}(\xi_{\rm in}) + \Delta j_{\nabla B}(\xi). \quad (23)$$

The radial gradient scale lengths of temperature and density are defined in terms of the radial transport coefficients in the SOL $\Delta_n = n_{\rm sep} D_\perp / \Gamma^{\rm sep}_\perp$, $\Delta_T = n_{\rm sep} T_{\rm sep} \chi_\perp / Q^{\rm sep}_\perp$, or they may be taken from experiment.

G. Solution for currents and potentials at target plates

Once the densities and temperatures are determined at the inner and outer divertor target plates [by solving Eqs. (1)–(13) in an iterative loop], Eqs. (14)–(23) can be solved for the electrostatic potentials and currents at the target plates. The current at the outer target can be evaluated from Eq. (23).

In general, the radial currents flowing across the separatrix are not radially ambipolar (radially divergence-free) at every poloidal, or parallel (ξ), location in the SOL and divertor. Only the total current (radial plus poloidal or parallel currents) is required to be divergence-free, as indicated explicitly in Eqs. (18), (19), and (23). In other words, parallel currents are set up to balance any divergence in the local radial current and maintain the SOL and divertor plasma quasineutral.

However, there remains also a requirement for quasineutrality of the core plasma inside the separatrix, which constitutes a requirement that the net radial current across the separatrix must vanish. (Note that this does not require that the radial current must vanish at every parallel location (ξ), but rather that the integral of the radial current crossing the separatrix taken over the entire separatrix vanishes; i.e., inward currents at one location can be compensated by outward currents at other locations to maintain quasineutrality of the core plasma.) The radial currents due to grad-B and curvature drifts are represented by the second term in Eq. (23), the integral over the separatrix of which will not vanish in general. This imbalance in the integrated radial current between the core and SOL must be balanced by radial currents driven by parallel viscosity, inertia, ion-neutral friction, perpendicular viscosity, etc.,[2] which phenomena are not included in the present model. It is intended to include other radial currents in a future version of this model. However, in the present model these additional radial currents are taken into account by an "integral-ambipolarity" condition consistent with maintenance of core plasma neutrality. This condition is imposed by adding or subtracting a constant to the term in square brackets in Eq. (23) that will cause the integral over the separatrix of the radial current between the core and SOL

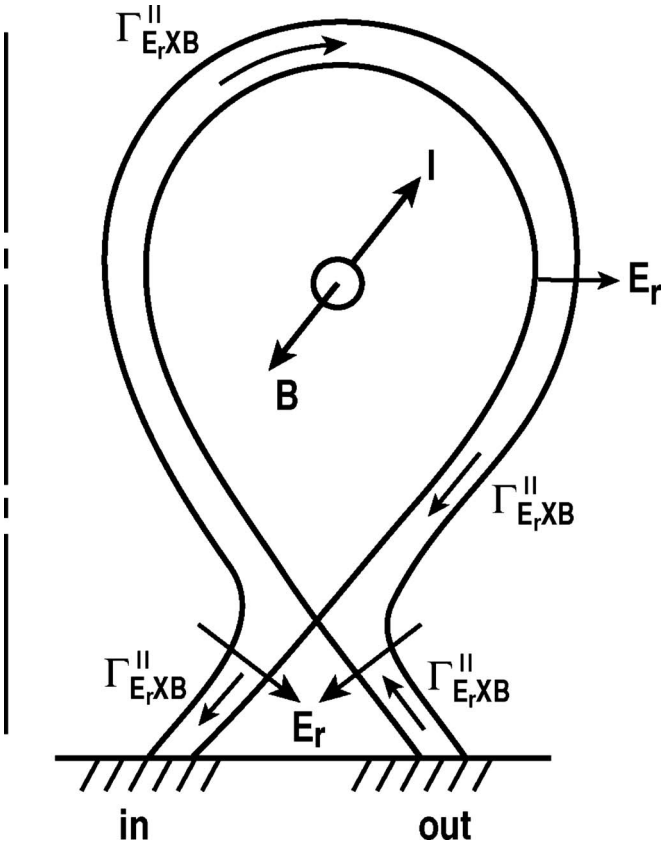

FIG. 4. Schematic of direction of radial electrostatic field $E_r = -\partial\phi/\partial r \sim -\partial T_e/\partial r$ and corresponding parallel $E\times B$ drift in SOL (inward temperature gradient) and divertor (outward temperature gradient) for $B(-)$ toroidal field direction.

to vanish (in effect the other radial currents are represented as being distributed uniformly over the SOL). This "integral-ambipolarity-constrained" current integral is represented by $\Delta\hat{j}_{\nabla B}(\xi)$. With this representation, Eq. (23) yields a relation between the currents into the plates at the inner and outer divertor targets

$$j_{\rm pl}^{\rm out} \equiv j_{\parallel}(\xi_{\rm out}) = j_{\parallel}(\xi_{\rm in}) + 2ne\Gamma^{\parallel}_{\nabla B}(\xi_{\rm out}) = -j_{\rm pl}^{\rm in} + 2ne\Gamma^{\parallel}_{\nabla B}(\xi_{\rm out}). \tag{24}$$

Equation (15) yields a relation between the potential just in front of the inner and outer plates

$$\phi_{\rm out} = \phi_{\rm in} + \frac{1.71}{e}[T_{\rm out} - T_{\rm in}] + \int_{\xi_{\rm in}}^{\xi_{\rm out}} \frac{T(\xi')}{en(\xi')}\frac{dn(\xi')}{d\xi'}d\xi' - \int_{\xi_{\rm in}}^{\xi_{out}} \frac{[j_{\parallel}(\xi_{\rm in}) + \Delta\hat{j}_{\nabla B}(\xi')]}{\sigma_{\parallel}(\xi')}d\xi'. \tag{25}$$

Using Eqs. (16) with $j_{\rm pl}^{\rm in} = -j_{\parallel}(\xi_{\rm in})$ and $j_{\rm pl}^{\rm out}$ given by Eq. (24) in Eq. (25) yields an equation that determines $j_{\parallel}(\xi_{\rm in})$. Note that although the integral of the radial currents over the SOL must vanish, the current integral in Eq. (25) is weighted by $1/\sigma_{\parallel} \sim 1/T^{3/2}$ and extends also over the divertor plasmas. This equation displays the well known result that the current in the SOL is driven by differences in potentials and temperatures at the target plates and by drifts due to the nonuniformity and curvature of the magnetic field (and other causes).

The above development has implicitly assumed that the target plates are at zero potential. If the plates are biased with respect to ground, then $\phi_{\rm in,out} \Rightarrow \phi_{\rm in,out} + \phi_{\rm in,out}^{\rm bias}$ in the above equations.

H. $E\times B$ drifts

Although $E\times B$ drifts do not produce currents, they do produce particle flows. The poloidal variation of the electrostatic potential produces an electric field and a corresponding "radial" $E\times B$ drift. This electric field is $\mathbf{E} = -\nabla\phi$, which, in general, has poloidal and radial components. We estimate this poloidal electric field and the resulting radial drift as

$$E_{\parallel} = -\left(\frac{d\phi}{d\ell_{\theta}}\right) \approx -\left(\frac{d\phi}{d\xi}\right), \quad v^{r}_{E_{\parallel}\times B} = \frac{\mathbf{E}\times\mathbf{B}}{B^2} = \frac{-\dfrac{d\phi}{d\xi}}{B} \tag{26}$$

directed as illustrated in Fig. 3 for the case in which the potential is negative in front of both target plates and increases to a maximum positive value at some point toward the top of the plasma in this model. Note that this electric field is in the poloidal direction, and the parallel subscript indicates its representation in the parallel coordinate system, as discussed in Sec. II A.

The radial $E\times B$ flows from the outboard divertor channel into the private flux region and from the private flux region into the inboard divertor channel will transfer ions from the outboard divertor channel across the private flux region beneath the plasma to the inboard divertor channel.[13]

The "radial drift" loss or gain of ions from both the SOL and the divertor channels can be represented by an $E\times B$ loss frequency

$$\nu_{E_{\parallel}\times B}(\xi) = \frac{v^{r}_{E_{\parallel}\times B}(\xi)}{\varepsilon\Delta_n}, \tag{27}$$

where Δ_n is an estimate of the "radial width" of the SOL calculated as discussed for Eq. (6) and $\varepsilon \approx 3$ is a flux surface expansion factor taking into account the widening of the SOL into the divertor channel. Assuming that some fraction $f_{E\times B}$ of the ions lost into the private flux region from the outboard divertor channel flow into the inboard divertor channel, the source density of ions to the inboard divertor channel may be represented

$$S^{\rm in}_{E_{\parallel}\times B} = \frac{f_{E\times B}\int_{\xi_{\rm out}}^{\xi_{X_{\rm out}}} \nu_{E_{\parallel}\times B}(\xi)n(\xi)d\xi}{\int_{\xi_{\rm in}}^{\xi_{X_{\rm in}}} d\xi}, \tag{28}$$

where $\xi_{X_{\rm out,in}}$ denotes the location of the X-point in the outer, inner SOL divertor.

The particle balance Eq. (4) in the divertor channels now becomes

$$\frac{d\Gamma}{d\xi} = \frac{\Gamma_{\perp}}{\Delta_n} + n_e(\nu_{\rm ion} - \nu_{\rm rec}) + n_i(\nu_{E_{\parallel}\times B} + \nu_B) + S^{\rm in}_{E_{\parallel}\times B}, \tag{29}$$

where the source term $S^{\rm in}_{E_{\parallel}\times B}$ is only present in the inboard divertor channel, for the field configuration shown in Figs.

1–4. The quantity ν_B is a radial transport frequency defined by an expression like Eq. (25) but using the radial curvature and grad-B drifts given by Eq. (20).

Positive radial drifts correspond to outward ion flow from the core into the SOL and constitute a source of ions to the SOL, while negative radial flows correspond to inward flows of ions from the SOL into the core and constitute a loss of ions in the SOL. In the divertor channels radial drifts in either direction constitute a loss of ions, and the radial drift frequencies in Eq. (29) are negative.

There is a radially outward directed electric field in the SOL produced by the radial temperature gradient in the SOL

$$E_r(\xi) = \frac{-d\phi}{dr} = -\phi\left(\frac{1}{\phi}\frac{d\phi}{dr}\right) \simeq -\phi\left(\frac{1}{T}\frac{dT}{dr}\right) \equiv \phi\Delta_T^{-1}, \quad (30)$$

which produces poloidal clockwise $E\times B$ drifts and particle fluxes in the SOL

$$v^{\theta}_{E_r xB}(\xi) = \frac{\phi(\xi)\Delta_T^{-1}}{B}, \quad \Gamma^{\theta}_{E_r xB}(\xi) = \frac{n(\xi)\phi(\xi)\Delta_T^{-1}}{B} \quad (31)$$

as illustrated in Fig. 4.

The representation of this poloidal particle flux in the parallel coordinate system constitutes a drift particle flux

$$\Gamma^{\parallel}_{E_r xB}(\xi) = \frac{B_\theta}{B}\Gamma^{\theta}_{E_r xB}(\xi) = \frac{n(\xi)\phi(\xi)\Delta_T^{-1}B_\theta}{B^2}, \quad (32)$$

which circulates clockwise around the SOL, as illustrated in Fig. 4.

The temperature distribution at the divertor target plate has been observed to peak somewhat outside the separatrix (i.e., to the right/left of the separatrix in the outer/inner divertor), causing the direction of the radial electric field along the separatrix to change from outward in the SOL to inward into the private flux region in the divertor channel. This produces a drift particle flux downward in the inner divertor and upward in the outer divertor, as illustrated in Fig. 4.

Both the drift particle fluxes [Eqs. (22) and (32)] are additive to the particle flux due to particle sources calculated from Eq. (29).

I. Diamagnetic drifts

The leading order local force balance on the plasma balances the pressure gradient with a $V\times B$ force, with the result that pressure gradients drive drift velocities orthogonal both to the field and the pressure gradient. In particular, a radial diamagnetic flow is driven by the pressure gradient in the direction perpendicular to the 2D strip in which the transport calculation of this paper is being carried out. This drift is represented as

$$v^{r}_{\mathrm{dia}} = \frac{-1}{neB}\frac{\partial p}{\partial \ell_\perp} \simeq \frac{-1}{neB}\frac{\partial p}{\partial \ell_\theta} \simeq \frac{-1}{neB}\frac{B}{B_\theta}\frac{\partial p}{\partial \xi}. \quad (33)$$

The radial pressure gradient also drives a diamagnetic drift velocity in the direction perpendicular to the 2D strip along the field lines of this calculation, but this drift is not considered in this calculation.

It has been shown[2] that the diamagnetic drift contributions produce currents and particle fluxes that are divergence-free except for small contributions due to field nonuniformities which are, in fact, the grad-B and curvature drift contributions. Thus, the above grad-B and curvature drift contributions represent the surviving diamagnetic drift contributions, and there are not additional explicit diamagnetic drift contributions in this calculation.

J. Total parallel ion flux

The total parallel ion flux is calculated by integrating the particle balance Eq. (29), including the radial transport and radial drift losses and sources, and adding the poloidal grad-B and $E\times B$ drift fluxes of Eqs. (22) and (32)

$$\Gamma(\xi) = \Gamma_{\mathrm{in}} + \left[\int_{\xi_{\mathrm{in}}}^{\xi} \frac{\Gamma_\perp^{\mathrm{sep}}}{\Delta_n} - \frac{D_\perp n}{\Delta_n^2} + n_e(\nu_{\mathrm{ion}} - \nu_{\mathrm{rec}}) + n_i(\nu_{E_\parallel\times B} + \nu_B + \nu_{\mathrm{dia}}) + S^{\mathrm{in}}_{E_\parallel\times B}\right] d\xi' + \Gamma^{\parallel}_{\nabla B}(\xi) + \Gamma^{\parallel}_{E_r\times B}(\xi), \quad (34)$$

with Γ_{in} given by the sheath boundary condition of Eq. (5) at the inner divertor target.

As before, the source term $S^{\mathrm{in}}_{E_\parallel\times B}$ only obtains in the inner divertor for the magnetic field geometry of Figs. 1–4.

K. Viscosity

Inclusion of parallel viscosity introduces a term

$$-\frac{d\pi}{d\xi} = \frac{d}{d\xi}\left(\eta\frac{dv}{d\xi}\right) = \frac{d}{d\xi}\left\{\eta\left[\nu_{\mathrm{ion}} - \nu_{\mathrm{rec}} + \frac{\Gamma_\perp}{n\Delta_n} - \frac{\Gamma}{n}\left(\frac{1}{n}\frac{dn}{d\xi}\right)\right]\right\} \quad (35)$$

on the right side of Eq. (8). This changes the solution for $M(\xi)$ of Eq. (9) to

$$M(\xi) = 4n_{\mathrm{in}}T_{\mathrm{in}} - \int_{\xi_{\mathrm{in}}}^{\xi} m\nu_{\mathrm{mom}}(\xi')\Gamma(\xi')d\xi' + \left\{\eta\left[\nu_{\mathrm{ion}} - \nu_{\mathrm{rec}} + \frac{\Gamma_\perp}{n\Delta_n} - \frac{\Gamma}{n}\left(\frac{1}{n}\frac{dn}{d\xi}\right)\right]\right\}_{\xi_{\mathrm{in}}}^{\xi}. \quad (36)$$

The Braginskii parallel viscosity coefficient $\eta = 1.96nT\tau_i$, $\tau_i = 3\sqrt{m_i}T^{3/2}/4\sqrt{\pi}n \ln\Lambda e^4$ is used.

Inclusion of cross-field viscous terms introduces additional cross-field currents, which would alter the parallel current calculated from Eq. (19). The usual practice is to attribute cross-field viscosity to anomalous processes represented by essentially a fitting parameter, but such terms are not included in the present model.

L. Neutral particle recycling

Neutral particle recycling and gas fueling effects on the SOL and divertor plasma are calculated with a simplified geometry 2D interface-current-balance model.[9] The atomic physics data used in the calculation are given in Ref. 14.

M. Impurities

The momentum balance equation (neglecting viscosity) for each individual impurity ion species, k, in a multispecies plasma can be written

$$\frac{d}{d\xi}(p_k + n_k m_k v_k^2) = z_k e n_k E_\parallel + R_{ke} + R_{ki}, \tag{37}$$

where e refers to electrons and i refers to the main plasma ion species. A similar equation obtains for the main ion species, with k and i interchanged and the atomic physics momentum loss term $-n_i m_i(\nu_{el,i}+\nu_{cx,i})v_i$ added to the right side. The momentum balance equation for the electrons (neglecting inertia and viscosity) is

$$\frac{d}{d\xi}(p_e) = -en_e E_\parallel + R_{ei} + \sum_k R_{ek}. \tag{38}$$

The collisional friction terms which appear in these equations are[15]

$$R_{ke} = \frac{n_k z_k^2}{n_i} R_{ie} = \frac{n_k z_k^2}{n_i}\left[\frac{-\eta_\parallel n_i e}{z_{\text{eff}}} j_\parallel + c_e^{(2)}\frac{n_i}{z_{\text{eff}}}\frac{dT}{d\xi}\right], \tag{39}$$

where

$$\eta_\parallel = \left[\frac{0.457}{1.077 + z_{\text{eff}}} + 0.29 z_{\text{eff}}\right] 2\sigma_\parallel^{-1},$$

$$c_e^{(2)} = 1.5\left(1 - \frac{0.6934}{1.3167^{z_{\text{eff}}}}\right) \tag{40}$$

and

$$R_{ki} = c_i^{(1)} n_i m_i \nu_{ik}(v_i - v_k) + c_i^{(2)}\frac{n_i}{z_{\text{eff}}}\frac{dT}{d\xi}, \tag{41}$$

where

$$\nu_{ik} = \frac{m_i + m_k}{m_k}\frac{4\sqrt{2\pi}\ln\Lambda e^4 z_k^2 z_i^2 n_k}{3\sqrt{m_i}T^{3/2}},$$

$$c_i^{(1)} = \frac{(1+0.24z_0)(1+0.93z_0)}{(1+2.65z_0)(1+0.285z_0)},$$

$$z_0 = \frac{\Sigma_k n_k z_k^2}{n_i}, \tag{42}$$

$$c_i^{(2)} = \frac{1.56(1+\sqrt{2}z_0)(1+0.52z_0)}{(1+2.65z_0)(1+0.285z_0)}\frac{1}{z_0 + \sqrt{(1+m_i/m_k)/2}}.$$

A particle continuity equation obtains for each ion species

$$\frac{d\Gamma_k}{d\xi} = S_k - \frac{D_{\perp k} n_k}{\Delta_n^2} + n_k(\nu_{E_\parallel xB,k} + \nu_{B,k} + \nu_{\text{dia},k}) + S^{\text{in}}_{E_\parallel xB,k}, \tag{43}$$

where the second term on the right represents transport loss perpendicular to the field lines and the first term represents the source of impurity particles, and the last two terms on the right represent the radial drifts of ions between the SOL and the core and the $E_\parallel \times B$ drifting of impurities from the outer to the inner divertor channel (in the geometry of this paper). For injected impurities, this source is just the local injection rate. For intrinsic impurities (e.g., carbon) this source density is $S_k = \Gamma_{\text{div},i} Y_{ik}/L_k$, where $\Gamma_{\text{div},i}$ is the incident main ion flux on the divertor target plate, Y_{ik} is the sputtering yield for target material k for ions of species i, and L_k is the distance along the field lines in front of the target plate over which the sputtered atoms become ionized (a centimeter or less).

The boundary conditions for the impurity ions are the sheath boundary condition on impurity ion velocity into the target plate at the sound velocity, $v_k = c_{sk} = \sqrt{2T/m_k}$, and the integral particle balance condition of the particle flux incident on the divertor targets

$$\begin{aligned}\Gamma_{\text{in},k} &= -(1-R_k^{\text{in}})n_{k,\text{in}}v_{k,\text{in}} \\ &= -(1-R_k^{\text{in}})\int_{\xi_{\text{in}}}^{\xi_{\text{stag}\Gamma}}\left(S_k - \frac{D_{\perp k}n_k}{\Delta_n^2} + n_k(\nu_{E_\parallel\times B,k} + \nu_{B,k} \right. \\ &\quad \left. + \nu_{\text{dia},k}) + S^{\text{in}}_{E_\parallel\times B,k}\right)d\xi, \\ \Gamma_{\text{out},k} &= (1-R_k^{\text{out}})n_{k,\text{out}}v_{k,\text{out}} \\ &= (1-R_k^{\text{out}})\int_{\xi_{\text{out}}}^{\xi_{\text{stag}\Gamma}}\left(S_k - \frac{D_{\perp k}n_k}{\Delta_n^2} + n_k(\nu_{E_\parallel\times B,k} + \nu_{B,k} \right. \\ &\quad \left. + \nu_{\text{dia},k}) + S^{\text{in}}_{E_\parallel\times B,k}\right)d\xi.\end{aligned} \tag{44}$$

The incident impurity ions are assumed to be recycled with reflection coefficient R_k as a return flux of impurity ions (i.e., ionization is assumed to take place immediately).

The total parallel impurity particle flux is obtained by integrating Eq. (43) and adding the grad-B and $E_\parallel \times B$ drift particle fluxes calculated as discussed above for the main ions but taking into account the difference in mass and charge.

$$\begin{aligned}\Gamma_k(\xi) &= \Gamma_{k,\text{in}} + \int_{\xi_{\text{in}}}^{\xi}\left(S_k - \frac{D_{\perp k}n_k}{\Delta_n^2} + n_k(\nu_{E_\parallel xB,k} + \nu_{B,k} \right. \\ &\quad \left. + \nu_{\text{dia},k}) + S^{\text{in}}_{E_\parallel xB,k}\right)d\xi + \Gamma^\parallel_{\nabla B,k}(\xi) + \Gamma^\parallel_{E_r\times B,k}(\xi).\end{aligned} \tag{45}$$

The momentum balance Eq. (37) can be integrated to obtain an equation for the impurity density distribution

$$\begin{aligned}&n_k(\xi)T(\xi) + m_k v_k(\xi)\Gamma_k(\xi) \\ &\quad = n_{\text{in},k}T_{\text{in}} + m_k v_{\text{in},k}\Gamma_{\text{in},k} + \int_{\xi_{\text{in}}}^{\xi} n_k(\xi')\left[-z_k e\frac{d\phi}{d\xi}\right. \\ &\qquad + z_k^2\left(\frac{c_e^{(2)}}{z_{\text{eff}}} + c_i^{(2)}\right)\frac{dT}{d\xi} - \frac{z_k^2\eta_\parallel e}{z_{\text{eff}}}j_\parallel \\ &\qquad \left. + c_i^{(1)} m_k \nu_{ki}\left(\frac{\Gamma_i}{n_i} - \frac{\Gamma_k}{n_k}\right)\right]d\xi'.\end{aligned} \tag{46}$$

Integrating the electron momentum balance of Eq. (38) yields an expression for the electrostatic potential that now explicitly accounts for impurities

$$\phi(\xi) = \phi_{\text{in}} + \frac{[1 + c_e^{(2)}\beta/z_{\text{eff}}]}{e}[T(\xi) - T_{\text{in}}] + \int_{\xi_{\text{in}}}^{\xi} \frac{T(\xi')}{en(\xi')}\frac{dn(\xi')}{d\xi'}d\xi' - \int_{\xi_{\text{in}}}^{\xi} \frac{\beta\eta_{\parallel}}{z_{\text{eff}}} j_{\parallel}(\xi')d\xi', \quad (47)$$

where $\beta = 1 + \sum_k n_k z_k^2/n_i / 1 + \sum_k n_k z_k/n_i$, and ϕ_{in} is given by the sheath relation of Eq. (16).

N. Solution procedure

The coupled set of nonlinear equations described above are solved numerically, using iterative procedures, the convergence of which is a somewhat delicate process. This solution procedure is incorporated in an integrated modeling code[16] which solves the core plasma power and particle balances to calculate the particle and heat fluxes $(\Gamma_{\perp}^{\text{sep}}, Q_{\perp}^{\text{sep}})$ flowing across the separatrix from the core into the SOL, the two-point equations for the divertor and SOL which provides the background plasma parameters for the neutral calculation, and the 2D transport of recycling neutrals. This calculation also provides starting conditions for the iterative solution.

III. EFFECTS OF DRIFTS ON THE DIVERTOR-SOL PLASMA DISTRIBUTIONS

As discussed above and as illustrated previously in a conglomerate way by calculations with the 2D fluid edge codes UEDGE (Refs. 1 and 17) and SOLPS,[2] particle drifts due to magnetic field gradients and curvature, electric fields, and pressure gradients have a major impact on determining the distribution of ion densities, temperature, ion flows, currents, electric fields, etc., in the divertor and scrape-off layer of tokamaks. The calculation of the previous section provides an excellent means for isolating and elucidating these effects, to which purpose a series of model problem calculations have been performed.

In order to ensure a realistic plasma edge regime, the model problem had machine and plasma core parameters of a DIII-D *H*-mode discharge, with two exceptions. The two divertor legs were symmetrized (i.e., made more like the figures above than the more asymmetric divertor configuration actually found in DIII-D) in order to avoid geometrical asymmetries that would otherwise additionally complicate the interpretation of the results of the calculations. In such a model problem, the solution in the absence of drifts should be symmetric. Second, the D-shape of the plasma was not retained in modeling the essentially vertical grad-B and curvature drifts, with the effect of making the radial and poloidal (parallel) components of these drifts of symmetric magnitude in the inner and outer SOL.

The model (R=1.7 m, a=0.6 m, κ=1.8, B=2.0 T, I=1.2 MA, q_{95}=4) represented a lower single null divertor plasma with the toroidal field such that the grad-B ion drift was down into the divertor; i.e., the configuration illustrated in Figs. 1–4. Another calculation was made in which the toroidal magnetic field direction was reversed. The power and particle fluxes into the SOL from the core plasma were calculated to match experimental conditions for an *H*-mode discharge.

The equations of the previous section were numerically integrated over a grid structure along the field lines from the inner to the outer divertor plates. A small (5 cm in the parallel dimension, about 1 cm in the poloidal dimension normal to the target plates) recycling region in front of each divertor plate, a prerecyling region of twice that length, and eight other regions represented each divertor channel up to and including the *X*-point region (total length of each divertor channel of 2.95 m along field lines). The SOL plasma from inner to outer *X*-points (parallel distance 53.02 m) was divided into 30 equal regions. With reference to Fig. 1, the recycling regions are 1 and 50, the inner and outer *X*-points are in regions 10 and 41, the inner and outer midplanes are in regions 18 and 33, and the "crown" at the top is regions 25 and 26. The symmetry point is between regions 25 and 26. All results will be plotted against region number. With the numerical integration scheme employed in this paper, the densities, temperature, and quantities constructed from them, such as the grad-B drift velocities, were calculated as average values over each region (e.g., the density shown in the following figures for location "1" is an average density over the first, recycling region in front of the inner divertor, and the density shown for location "33" is an average over the region containing the outer SOL midplane). However, quantities such as the parallel particle fluxes and particle velocities, parallel currents, electrostatic potential and associated electric fields and $E \times B$ drift velocities were calculated at the interfaces between regions (e.g., the currents and velocities shown for location 1 are the values at the inner divertor target plate, the currents and velocities shown for location "26" are the values at the symmetry point between regions 25 and 26, and the currents and velocities shown for location "51" are the values at the outer divertor plate).

Particle sources were treated as follows. The gas fueling source for the deuterium (1.5×10^{20}#/s into the upper outboard plasma chamber) was represented explicitly, and the resulting neutral atoms were transported through the edge region across the separatrix to fuel the core plasma. An average ion flux of $\Gamma_{\perp} = 1.6 \times 10^{20}$#/m^2 s from the core plasma into the SOL was calculated, taking into account this neutral influx into the core, but consisting mostly of ions produced by the neutral beam particle source. The deuterium ions striking the target plates (consisting both of ions crossing the separatrix from the core and ions produced by ionization of neutral atoms in the SOL and divertor) were reflected as neutral atoms at about one-half their incident energy or reemitted as molecules which were dissociated into 2 eV atoms in the recycling regions 1 and 50 and were then transported throughout the edge region until ionized in the divertor, SOL, or plasma edge inside the separatrix.

Two impurity ion species were modeled: carbon, which is an intrinsic impurity, and argon, which is sometimes injected to enhance radiation. The carbon source was the calculated sputtering of the deuterium ions incident on the di-

vertor target plates and was distributed over the first two regions (i.e., 1 and 2, 49 and 50) in front of the target. Carbon ions returning to the target plates were reflected with a coefficient $R=0.99$, which included in an approximate manner also the effects of carbon self-sputtering. An argon source of 2×10^{19}#/s injected in the private flux region was assumed to be pumped by the divertor plasma and was represented as a uniformly distributed particle source in the two divertor plasmas (regions 1-9 and 42-50). The argon ions incident on the divertor targets were reflected with coefficient $R=0.99$. Carbon and argon were each transported as a single ion species with an average charge state that varied with local electron temperature along the field lines.

An average heat flux of $Q_\perp=8.\ 8\times10^4$ W/m^2 into the SOL from the core plasma was calculated from a core power balance, taking into account the 4.9 MW neutral beam heating, the small Ohmic heating and the radiation from inside the separatrix. Both this heat flux and the above ion flux into the SOL from the core were uniformly distributed over the SOL regions 11-40.

Radial transport was represented by a gradient scale length of 2 cm for density and temperature.

A. Drifts

The radial and parallel grad-B, $E\times B$ and diamagnetic drifts for the deuterium ions calculated for the magnetic configuration of Figs. 1–4, with toroidal magnetic field in the opposite direction to the plasma current, were calculated. The total parallel particle flux, taking into account these drifts as well as the ion flux into the SOL from the core, was also calculated. The diamagnetic drifts are very large just in front of the divertor plates where the parallel pressure gradients are large, but otherwise the grad-B drifts are the most important.

Three different situations were calculated for the sake of comparison: (i) with the grad-B, $E\times B$ and diagmagnetic drifts turned off, (ii) with these drifts turned on and the toroidal magnetic field in the direction opposite to the plasma current shown in Figs. 1–4, denoted $B(-)$, and (iii) with the drifts turned on and the toroidal magnetic field reversed and aligned with the current opposite to the direction shown in Figs. 1–4, denoted $B(+)$.

B. Density and temperature distributions

The calculated densities and temperatures are shown in Figs. 5 and 6, respectively. The drifts do not have much effect on the deuterium density and temperature distributions, except in the recycling regions 1 and 50, where the diamagnetic and $E\times B$ drifts are large. The $E\times B$ drifts of Eq. (30) are largest near the divertor target plates because the electrostatic potential increases most rapidly there, and the diagmagnetic drifts are also largest near the divertor target plates, but because the parallel pressure gradients are largest there. The effect of drifts on the carbon and argon density profiles is greater than on the deuterium density profile.

With reference to Eqs. (10) and (11), the density profile is determined by the force balance requirement that the pressure plus inertial forces are constant over the SOL and divertor except for the momentum dissipation, which takes place for the deuterium ions primarily via atomic physics collisions with neutrals in the divertor. For the parameters of this calculation, for which the pressure in the SOL is almost 1000 Pa, the pressure term dominates the force balance, and the drift effects, which enter the density calculation via the inertial term in the force balance, have minimal effect except in the divertor, particularly in the recycling regions. The effect of drifts on the temperature profile is via the density profile and is correspondingly small in this problem, again except in the recycling regions. A greater sensitivity to drifts was found in a similar comparison[2] for which the pressure was an order of magnitude lower in the SOL; such a sensitivity would result in this calculation also if the pressure contribution to the M term in Eq. (11) was decreased by an order of magnitude.

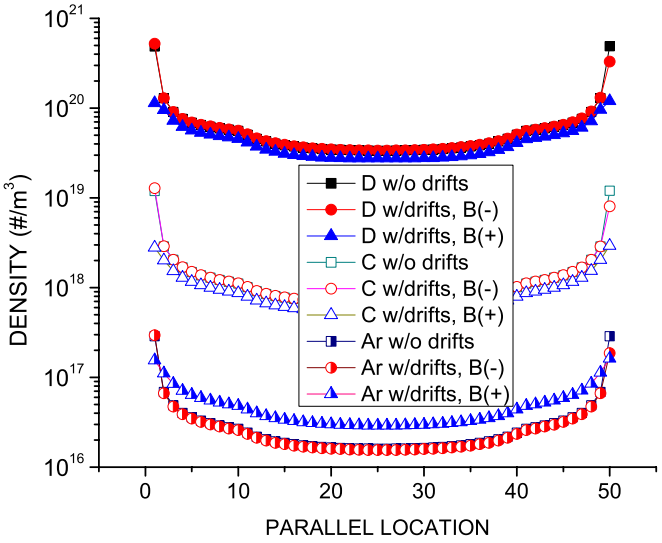

FIG. 5. (Color online) Deuterium, carbon, and argon ion densities in divertor (locations 1-9 and 42-50).

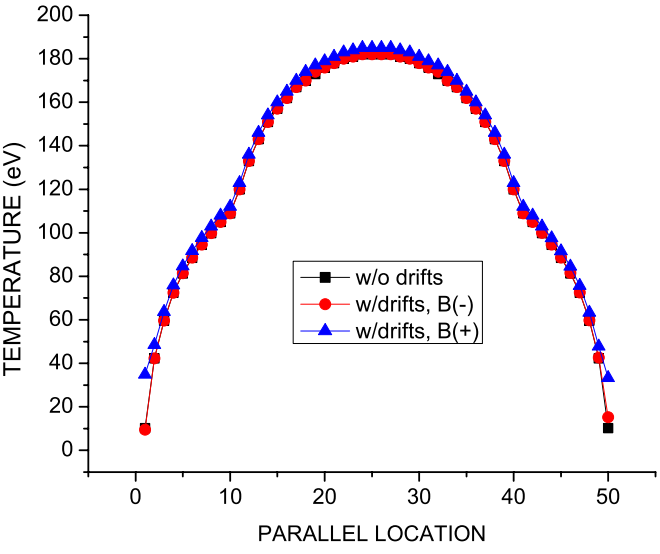

FIG. 6. (Color online) Temperature distribution in divertor (regions 1-9 and 42-50) and SOL.

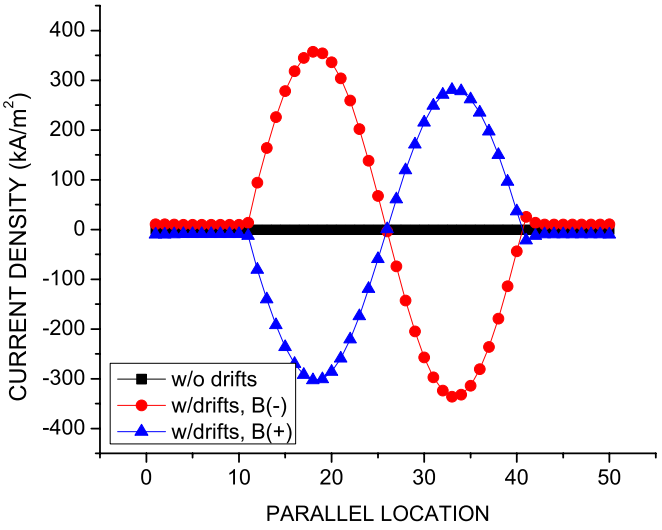

FIG. 7. (Color online) Parallel plasma current density in divertor (regions 1-9 and 42-50) and SOL.

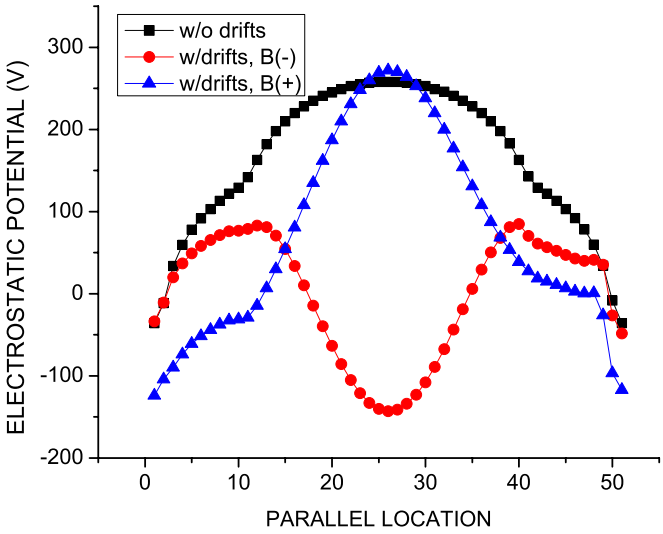

FIG. 8. (Color online) Electrostatic potential distribution in divertor (regions 1-9 and 42-50) and SOL.

C. Electrical current density, potential, and fields

The grad-B and curvature drifts produce radial currents proportional to the grad-B and curvature drifts given by Eq. (21) and indicated in Fig. 2. Without drifts, the temperature distribution was symmetric and there was no thermoelectric current. With the $B(-)$ drifts, there was a temperature asymmetry that drove a thermoelectric current and large radial grad-B drift currents that drove parallel currents in order to maintain a divergence-free total current density. These radial grad-B currents and the compensating parallel currents were in opposite directions for the $B(-)$ and $B(+)$ field directions. Note that the grad-B currents integrated to zero over the SOL to maintain ambipolarity, as discussed in connection with Eq. (23). Scrape-off layer currents of comparable magnitude have been measured in DIII-D H-mode discharges,[18] but we are unaware of any measurements of current profiles in the SOL.

With the drifts turned off, the symmetric temperature and density distributions shown in Figs. 6 and 5 result in the symmetric parallel current distribution shown in Fig. 7 and the symmetric electrostatic potential distribution shown in Fig. 8, as calculated from Eq. (15) using Eqs. (16), (24), and (25). Turning on the grad-B drift and changing the direction of the toroidal magnetic field both produce a dramatic change in the parallel distribution of the electrostatic potential, primarily because to the differences in the parallel currents shown in Fig. 7.

Differentiation of the electrostatic potential profiles of Fig. 8 produces the poloidal electric fields of Eq. (26). These fields are generally small in the SOL but become quite large in the divertors, particularly in the vicinity of the target plates.

As discussed in connection with Eq. (30), the implication of Eq. (15) is that the radial gradient of the electrostatic potential (the radial electric field) should be approximately proportional to the radial temperature gradient, which is characterized by the parameter $\Delta_T^{-1}=-dT/Tdr$. Using $\Delta_T=2$ cm and the temperature profiles of Fig. 6, Eq. (30) yields radial electric fields which are quite different with and without drifts, primarily because of the difference caused in the electrostatic potentials of Fig. 8 by the differences in parallel current distributions shown in Fig. 7. For the $B(-/+)$ field direction, the positive/negative radial electric field in the SOL corresponds to the temperature decreasing radially outward from the separatrix. In the divertor, the experimental evidence is that the peak in the temperature profile just in front of the target is somewhat outside the separatrix, so that at the separatrix there is a transition from a "negative" temperature gradient in the SOL to a positive temperature gradient at the target plate, leading to an oppositely directed radial electric field into the private flux region.

D. Parallel flows

In the absence of drifts, because of the symmetry of the geometry and of the particle source from the core plasma into the SOL, the particle flows go symmetrically to the inner and outer divertor targets, as shown for D in Fig. 9. The sputtered particle sources in front of the divertor targets for C are also symmetric, and the resulting C particle fluxes are symmetric in the absence of drifts, as shown in Fig. 10. For D, the principle source of ions is the particle flux $\Gamma_\perp^{sep}$ from the core, although there is a smaller source due to ionization of neutrals (primarily in the divertor). Without drifts, flow stagnation is at the symmetry point (between regions 25 and 26) at the crown of the SOL, as shown for D in Fig. 9. For C the source is the sputtered carbon from the divertor plates deposited uniformly in the first two regions (1 and 2, 50 and 49), which is basically entrained in the high deuterium flow toward the plates in these regions.

Turning the drifts on produces two types of effects. First, the poloidal $E\times B$ and grad-B drifts of Eqs. (32) and (22) produce a local increase or decrease in particle parallel flow velocity. Second, the outward and inward radial particle drifts of Eqs. (20), (26), and (33) produce sources and sinks of particles in the SOL and divertor, which affect the parallel particle flux as indicated by Eqs. (34) and (45). The parallel

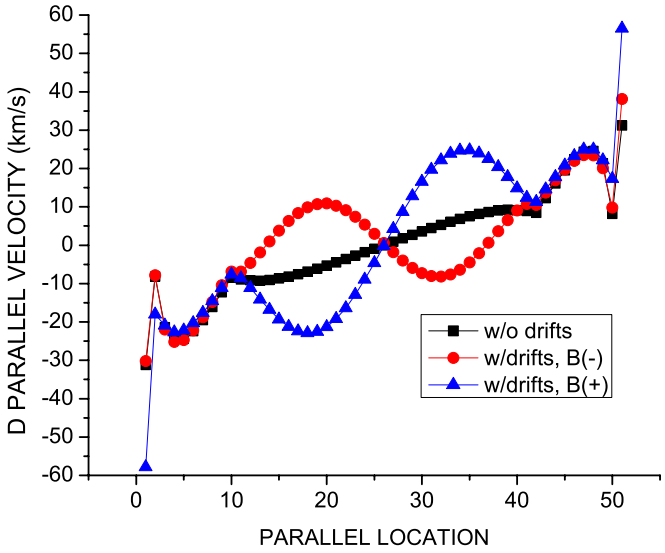

FIG. 9. (Color online) Parallel deuterium ion velocity in divertor (regions 1-9 and 42-50) and SOL.

deuterium ion flux must increase or decrease in response to this variation in ion sources and sinks to satisfy the continuity equation. The momentum balance equation is dominated by the pressure term in the SOL, which produces the relatively flat ion distribution over the SOL, so the variation in ion flux requires the variation in deuterium parallel velocity shown in Fig. 9.

With reference to Figs. 2 and 3 for the $B(-)$ field direction, both the grad-B and $E\times B$ radial drifts are out of the core, providing a particle source in the SOL between the X-point (region 10) and the midplane (region 18) of the inner SOL. Between the midplane (region 18) and the crown (region 25) the grad-B drift is inward and the $E\times B$ drift is outward, providing a sink and a source, respectively, of particles to the SOL. Between the crown (region 26) and the midplane (region 33) of the outer divertor both drifts are inward from the SOL into the core, providing a particle sink in the SOL. From the midplane (region 33) to the X-point (region 41) the grad-B drift is outward and the $E\times B$ drift is inward, proving a source and a sink, respectively, of particles to the SOL. The diagmagnetic drift is relatively smaller in the SOL. The particle flux variation in the SOL for deuterium for the $B(-)$ field direction shown in Fig. 9 reflects this variation in particle source and sink distributions.

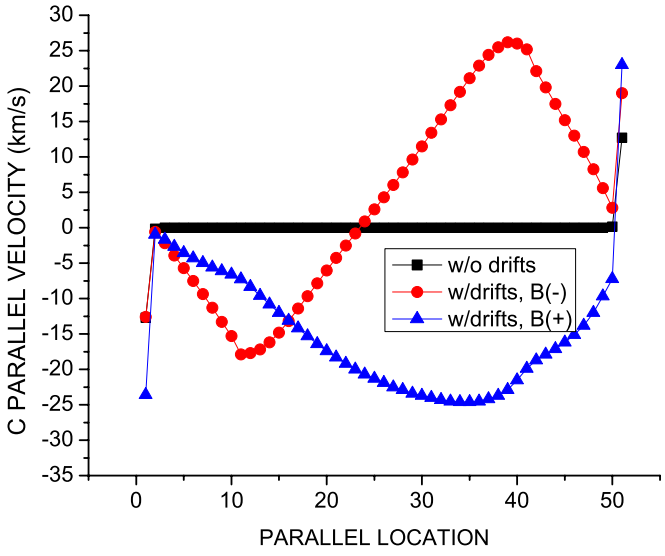

FIG. 10. (Color online) Parallel carbon ion velocity in divertor (regions 1-9 and 42-50) and SOL.

Note that there are three stagnation points in the deuterium parallel flow in the SOL for the $B(-)$ drifts. Recent probe measurements of deuterium flow in DIII-D (Ref. 19) and Alcator C-MOD (Ref. 20) find similar results. In a DIII-D L-mode discharge with the same $B(-)$ field direction (grad-B drift toward divertor), probe measurements found a similar magnitude of deuterium flow in the crown region and also two flow stagnation points.[19]

In a C-MOD discharge comparable to the B-case shown in Fig. 9 (grad-B drift toward lower divertor) discharge, four probe measurements near the outboard midplane found parallel ion flows toward the inboard divertor, consistent with the negative flows calculated for locations 30-35 shown in Fig. 9. The single inboard midplane probe measurement for C-MOD also found a negative flow toward the inner divertor, while the calculation shown in Fig. 9 at location 18 predicts stagnant or slightly positive flow, but the differences in configuration and plasma condition could easily account for this difference. The C-MOD experiment did not have probes in the upper inboard quadrant that could have detected the predicted positive flow toward the outboard divertor. Note that the positive/negative sign convention for the parallel flows is reversed for this paper and for the C-MOD results. Further note that the current and field are usually parallel in CMOD and are both reversed when the field is reversed, as contrasted to the situation calculated in this paper in which the current and field are antiparallel for the $B(-)$ case and only the field is reversed to obtain the $B(+)$ case, so that the calculated current and electrostatic potential results do not apply to CMOD.

The C-MOD parallel flow results were originally attributed[20] to a ballooning mode enhancement of particle transport from the core into the SOL on the outboard side. Subsequently, Aydemir[21] offered an explanation for the C-MOD parallel flow results somewhat similar to the model of this paper, but based on poloidally asymmetric ion sources and sinks in the SOL due to radial Pfirsch–Schluter flows from and to the core, instead of the poloidally asymmetric ion sources and sinks in the SOL due to grad-B and curvature drifts from and to the core that are modeled in this paper. These Pfirsh–Schluter flows would be radially outward from the core into the SOL on the outboard low-field side and radially inward from the SOL to the core on the inboard side. The grad-B effect is capable of producing multiple stagnation points, as shown in Fig. 9 (for the $B+$ case), but neither the ballooning mode nor the Pfirsch–Schluter effect is capable of doing this, so several probe measurements of parallel ion flow in the inboard SOL could distinguish between the "grad-B drift" explanation on one hand and "ballooning mode" or "Pfirsch–Schluter" explanations on the other hand.

When the field direction is changed from $B(-)$ to $B(+)$

all of the radial drift directions are reversed, reversing the particle source and sink distributions in the SOL. The changes in the sources and sinks in the divertor channels are not as pronounced. The resulting deuterium ($B+$) velocities are shown in Fig. 9

The calculated carbon parallel flow distributions are shown in Fig. 10. The same type of variation in particle sources and sinks because of the radial drifts also is present for carbon, but obviously other factors are dominant in the carbon force balance because the carbon parallel flows are of the opposite sign from the deuterium parallel flows in many locations. This opposite signs for the carbon velocity (which can be measured) and the deuterium velocity (which cannot) has profound implications for the interpretation of flow measurements in the SOL.

E. Penetration of injected argon into the core plasma

It has been observed experimentally[22] in DIII-D H-mode discharges that the penetration of the core plasma by argon injected into the private flux region of the divertor is significantly greater when the ion grad-B drift is toward the divertor $[B(-)]$ than away from the divertor $[B(+)]$. In the model of this paper, the net penetration of argon from the SOL into the core can be characterized by the parameter $\int_{\xi_{X_{\mathrm{in}}}}^{\xi_{X_{\mathrm{out}}}} n_{\mathrm{Ar}}(v_{E_{\parallel}\times B,\mathrm{Ar}}^{r}+v_{B,\mathrm{Ar}}^{r}+v_{\mathrm{dia,Ar}}^{r})d\xi<0$, indicating a net radially inward $(-)$ drift. This parameter is calculated to be <0 for the $B(-)$ field direction shown in the Figs. 1–4, with the ion grad-B drift direction into the divertor, and to be >0 for the reversed $B(+)$ field direction with the ion grad-B drift direction out of the divertor, in qualitative agreement with the experimental observation. The significantly lower argon density shown in the divertor and SOL in Fig. 5 for the $B(-)$ than the $B(+)$ magnetic field configurations is also indicative of this same trend; since both calculations were performed with the same argon source and recycling coefficient, the lower argon concentration in the SOL for $B(-)$ than for $B(+)$ indicates a larger argon concentration in the core (by a factor of 2–3).

IV. SUMMARY

A calculation was made of the effects of drifts and toroidal magnetic field direction on flows, currents, electric fields, density, and temperature distributions in a model problem with parameters characteristic of a DIII-D H-mode discharge. A number of interesting phenomena—multiple reversal of parallel flows and currents in the SOL, opposite signs of the carbon and deuterium flow velocities in the SOL, reversal of the sign of the electrostatic potential and electric fields with the reversal of the toroidal magnetic field direction, larger penetration of the core plasma by argon injected in the divertor when the ion grad-B drift was toward than away from the divertor, etc., were predicted, many of which have been experimentally observed.

ACKNOWLEDGMENTS

The author would like to express his appreciation to R. Isler, R. Groebner, M. Groth, T. Petrie, M. Schaeffer, and G. Staebler for discussion of various aspects of this work and to General Atomics for hosting him during much of it. This work was supported by the U.S. Department of Energy under Grant No. DE-FG02-00-ER54538 with the Georgia Tech Research Corporation.

[1] T. D. Rognlien, D. D. Ryutov, N. Mattor, and G. D. Porter, Phys. Plasmas **6**, 1851 (1999); Contrib. Plasma Phys. **38**, 152 (1998); Plasma Phys. Controlled Fusion **47**, A283 (2005).
[2] V. A. Rozhansky, S. P. Voskoboynikov, E. G. Kaveeva, D. P. Coster, and R. Schneider, Nucl. Fusion **41**, 387 (2001); **42**, 1110 (2002); **43**, 614 (2003); Contrib. Plasma Phys. **46**, 575 (2006).
[3] G. M. Staebler, Nucl. Fusion **36**, 1437 (1996).
[4] M. J. Schaffer, A. V. Chankin, H. Y. Guo, G. F. Matthews, and R. Monk, Nucl. Fusion **37**, 83 (1997).
[5] G. J. Radford, A. V. Chankin, G. Corrigan, R. Simonini, J. Spence, and A. Taroni, Contrib. Plasma Phys. **36**, 187 (1996).
[6] R. Zagorski, H. Gerhauser, and H. A. Claassen, Contrib. Plasma Phys. **38**, 61 (1998).
[7] J. Luxon, Nucl. Fusion **42**, 614 (2002).
[8] W. M. Stacey, Phys. Plasmas **16**, 032506 (2009).
[9] W. M. Stacey, Nucl. Fusion **40**, 965 (2000).
[10] K. C. Shaing, Phys. Rev. Lett. **63**, 2369 (1989).
[11] T. D. Rognlien, P. N. Brown, and R. B. Campbell, Contrib. Plasma Phys. **34**, 362 (1994).
[12] F. L. Hinton and Y.-B. Kim, Nucl. Fusion **34**, 899 (1994).
[13] M. J. Schaffer, B. D. Bray, J. A. Boedo, T. N. Carlstrom, R. J. Colchin, C.-L. Hsieh, R. A. Moyer, G. D. Porter, T. D. Rognlien, J. G. Watkins, and DIII-D Team, Phys. Plasmas **8**, 2118 (2001).
[14] W. M. Stacey and E. W. Thomas, Phys. Plasmas **4**, 678 (1997); **2**, 3740 (1995).
[15] M. Keilhacker, R. Simonini, A. Taroni, and M. L. Watkins, Nucl. Fusion **31**, 535 (1991).
[16] W. M. Stacey, Phys. Plasmas **5**, 1015 (1998).
[17] G. D. Porter, S. L. Allen, M. Brown, M. E. Fenstermacher, D. N. Hill, R. A. Jong, A. W. Leonard, D. Nilson, M. E. Rensink, T. D. Rognlien, and G. R. Smith, Phys. Plasmas **3**, 1967 (1996).
[18] M. J. Shaeffer, personal communication (July 2008).
[19] M. Groth, G. D. Porter, J. A. Boedo, N. H. Brooks, R. C. Isler, W. P. West, B. D. Bray, M. E. Fenstermacher, R. J. Groebner, A. W. Leonard, R. A. Moyer, T. D. Rognlien, J. G. Watkins, and J. H. Yu, "Measurements and simulations of scrape-off layer flows in the DIII-D tokamak," Plasma Surface Interaction Conference, Toledo, 2008, J. Nucl. Mater. (to be published).
[20] B. LaBombard, J. E. Rice, A. E. Hubbard, J. W. Hughes, M. Greenwald, F. S. Granetz, J. H. Irby, Y. Lin, B. Lipschultz, E. S. Marmar, K. Marr, D. Mossessian, R. Parker, W. Rowan, N. Smick, J. A. Snipes, J. L. Terry, S. M. Wolfe, S. J. Wukitch, and the Alcator C-MOD team, Phys. Plasmas **12**, 056111 (2005).
[21] A. Y. Aydemir, Phys. Plasmas **14**, 056118 (2007).
[22] T. W. Petrie, N. H. Brooks, M. E. Fenstermacher, M. Groth, A. W. Hyatt, R. C. Isler, C. J. Lasnier, A. W. Leonard, G. D. Porter, M. J. Schaffer, J. G. Watkins, M. R. Wade, and W. P. West, Nucl. Fusion **48**, 045010 (2008); also Plasma Surface Interaction Conference, Toledo, 2008, J. Nucl. Mater. (to be published).